Soft Matter

Accepted Manuscript

ROYAL SOCIETY OF CHEMISTRY

www.rsc.org/softmatter

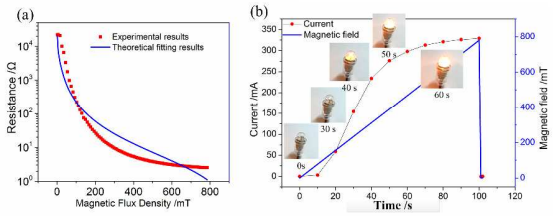

Tremendously improved conductivity of GMRP by graphite doping and the magnetic field dependent electro-conductivity enable GMRP as a smart switch.

Cite this: DOI: 10.1039/c0xx00000x

www.rsc.org/softmatter

PAPER

Magnetic Field Dependent Electro-conductivity of the Graphite Doped Magnetorheological Plastomer

Haoming Pang,[a] Shouhu Xuan,*[a] Taixiang Liu,[a] Xinglong Gong*[a]

Received (in XXX, XXX) Xth XXXXXXXXX 20XX, Accepted Xth XXXXXXXXX 20XX

DOI: 10.1039/b000000x

This work reported a novel graphite doped conductive magnetorheological plastomer (GMRP) with magnetic field dependent electro-conductivity. The conductivity of the GMRP increased by increasing the content of the graphite particles, while it decreased with the graphite size. When the graphite content reached to 15 wt%, the conductivity of GMRP is approximately 10000 times higher than the non-doped MRP. Because the iron particles in the GMRP were magnetic, the conductivity of the GMRP was magnetically sensitive. Under applying a 780 mT magnetic field, the electric conductivity could increase about 1000 times larger than the one under zero magnetic field. A particle-particle resistance model was developed to investigate the influence of the magnetic field and graphite doping on the conductivity, and the fitting curve matched the experimental results very well. Finally, a magnetically controllable on-off switch based on GMRP was proposed and its working mechanism was discussed.

1. Introduction

As a new kind of smart material, magnetorheological (MR) plastomer was prepared by dispersing micro-sized magnetically soft particles into a weak cross-linked polymer matrix [1, 2]. Different from the traditional MR gel, magnetorheological plastomer (MRP) is a solid-like gel and behaves like a plasticine. It can be moulded into various shapes and the shapes can be kept for a long time. Different to the MR fluid, no sedimentation of carbonyl iron powders (CIP) was found in MR plastomer because of the high viscosity of the matrix. Under applying an external magnetic field, the magnetically soft particles would overcome the constraint of the matrix and rearrange into a strings-like structure. After removing the magnetic field, these microstructures would be well kept. Because of these unique structural characteristics, the MRP was more stable than MR fluid [3-5] and presented a higher magnetorheological effect than the MR elastomer (MRE) [6-8]. To this end, they were very promising for practical applications, such as energy absorbers and vibration isolators [9, 10].

Since the CIPs were conductive, the MR materials were also conductive polymer composite (CPC) [11, 12] materials which were usually prepared by mixing the conductive particles into an insulating phase. Distinctively, the column-like aggregated microstructures of CIPs also enable the MR materials exhibit typical stimuli dependent conductivity [13-15]. Martin et al reported a high performance conductive nanocomposite by dispersing gold-coated magnetic particles in a polymeric resin [16, 17]. It was found that the nanocomposites were very sensitive to small volume changes, and their resistance could change ten orders of magnitude with the strain increased from 0 to 7%. Kchit and Bossis performed a systematical study on conductive mechanism in MRE and they presented that the resistance of MRE mainly comes from the interface, such as the roughness parameter, the thickness of the oxide layer and the thickness of the polymer layer [18]. Wang used impedance spectroscopy method to investigate the impedance and resistance of MRE. Simultaneously, a phenomenological model was proposed to understand the impedance response of MREs under different mechanical loads and magnetic fields [19]. Recently, Ghafoorianfar et al studied the sensing capabilities of magnetorheological elastomers by combining the effects of magnetic fields and mechanical compression loads [20]. The finite element analysis indicated that the coupled magnetostriction and magnetoresistance determined the piezoresistivity effect of MREs under the combined loading condition.

The conductivity of the MRP was very sensitive to the external magnetic field due to the position of the CIP was magnetically movable. Different from the traditional MRE, the MRP possessed a large change region in the conductivity because the CIPs in the MRP could be ranged from isotropic to anisotropic. Xu et al demonstrated that the inner structure of MRP exhibited a big influence on samples' resistance using impedance spectroscopy method [21] and the influence of particle chain direction on the conductivity of anisotropic MRP was investigated. Based on the structural dependent conductivity, an equivalent method was developed to quantitatively characterize the anisotropy of MRP. Such a magnetically sensitive conductivity was much favourable for their application such as the on-off switch. Unfortunately, since the obstacle of the polymer layers, the resistance in the CIP aggregated columns was still very high [22], more work should

be done to improve the conductive sensitivity of the MRP.

The addition of the conductive doping is the most common method for improving the conductivity of the MR materials [23-25]. Li et al developed the high performance MREs with excellent mechanical and electrical properties by using graphite as the additive [26, 27]. In their model, the current flowing through the chain structure consisted of both a tunnel current and a conductivity current, both were dependent on the external loadings. Bica et al. have done several meaningful works in this area and they found the doped MR materials exhibited typical magnetic dependent conductivity and capacity [28]. Some other doping like silvers, graphene and carbon nanotubes [29, 30] or other matrix like ionic liquids and ion gels [31-33] can also improve the conductivity of MR materials [34, 35]. In consideration of their unique structural characteristic, the MRPs enhanced by the conductive doping must be much useful in the sensor and energy areas [36-38]. However, few works have been developed to study the relativity between the resistance and the external magnetic field for the doped MRPs. Moreover, the magnetic dependent conductive model was much helpful for not only understanding the conductive mechanism but also predicting the conductive properties during the application. Therefore, the development of high conductive MRP and studying their stimuli dependent conductivity in both experiment and theory become an important point in this area.

In this work, a novel magnetic field dependent electro-conductive MRP doped with graphite (GMRP) was developed. The conductivity of the GMRP was tunable by varying the content and size of the graphite doping. Under the optimum condition, the GMRPs present well-defined magnetically responding conductivity and the coupling characteristic can be described by using a particle-particle resistance model. A possible mechanism was proposed to demonstrate the high sensitivity of the GMRPs. Finally, a simple on-off switch was developed and the results indicated that such smart materials had widely potential in smart device.

2. Experimental

2.1 Sample Preparation

The materials used for the GMRPs are: toluene diisocyanate (TDI, 2,4-TDI at ~80%, 2,6-TDI at ~20%, Tokyo Chemical Industry Co. Ltd, Japan), polypropylene glycol (PPG-1000, Sinopec Group Co. Ltd, China), 1,4-Butanediol (BDO, Sinopharm Chemical Reagent Co., Ltd, China), carbonyl iron powder (CIP, type CN, BASF aktiengesellschaft, Germany) and flake graphite powder (FGP, Dongguan Xieli graphite products Co. Ltd, China). The FGPs are of three different particle sizes (13.0 μm, 6.5 μm and 2.6 μm). The average diameter of the CIPs is about 6.0 μm.

GMRP samples with different CIP concentrations, FGP concentrations and FGP sizes are prepared by using homemade polyurethane (PU) as the matrix. To synthesize polyurethane, the TDI and PPG were added to a flask with the molar ratio 3:1 at 80 °C for 2 hours. Their weights were calculated by the formula bellow:

$$\frac{m_{TDI}/174g\cdot mol^{-1}}{m_{PPG}/1000g\cdot mol^{-1}}=3.$$

Later, BDO was added into the reactor and the temperature was set at 60 °C for about 40 minutes. The weight of BDO was calculated by the formula bellow:

$$\frac{m_{TDI}/174g\cdot mol^{-1}}{m_{PPG}/1000g\cdot mol^{-1}+m_{BDO}/90g\cdot mol^{-1}}=1.1.$$

The reaction was kept under stirring. As soon as the reaction was completed, the CIPs and FGPs were added under vigorously mixing before the temperature was cooling down.

In our experiment, three groups of GMRPs were prepared and the compositions of all GMRPs were shown in table 1. Group 1 are samples with different FGP concentrations. The size of the FGPs were 6.5 μm and their CIP's weight ratio were 70 wt%. These samples were defined as MRP-0, MRP-5, MRP-10, and MRP-15, respectively. The number means the weight of FGP in 100 g matrix and their volume fraction are 0%, 1.9%, 3.6% and 5.3%. Group 2 are samples with different CIP concentrations. Their CIPs' weight ratios are 50 wt%, 60%, 70% and 80% corresponding to 11%, 16%, 23%, and 34% in volume fraction respectively. They were named as MRP-50, MRP-60, MRP-70, and MRP-80, respectively. Group 3 are samples doped FGPs with different sizes, while the other parameters are kept constant, e.g. 5 g of 6.5 μm FGPs in 100 g matrix. The diameters of the FGPs are varied from 13.0 μm to 6.5 μm and 2.6 μm, thus the relative samples were named as MRP-13.0, MRP-6.5 and MRP-2.6.

Table 1 Compositions of GMRP samples.

Sample no.	Group 1				Group 2				Group 3		
	1	2	3	4	5	6	7	8	9	10	11
PU (g)	10	9.5	9.0	8.5	9.5	9.5	9.5	9.5	9.5	9.5	9.5
FGPs (g)	0	0.5	1.0	1.5	0.5	0.5	0.5	0.5	0.5	0.5	0.5
FGP sizes (μm)	6.5	6.5	6.5	6.5	6.5	6.5	6.5	6.5	13	6.5	2.6
CIPs (g)	23	23	23	23	10	15	23	40	23	23	23

2.2 Experimental Setup

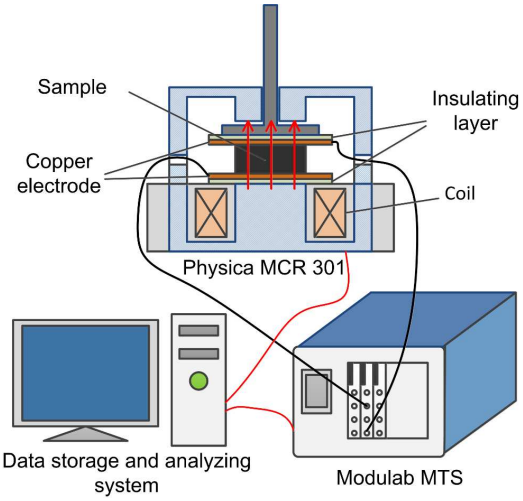

Figure 1. Schematic of experiment setup for the resistance measurements of GMRP.

Figure 1 shows the schematic of the experimental setup used to characterize the magnetic field dependent conductivity of the GMRPs. The system consists of three parts: a commercial rheometer Physica MCR301 (produced by Anton Paar GmbH, Austria) equipped with an electro-magnetic accessory MRD180, Modulab material test system (MTS, Solartron analytical, AMETEK advanced measurement technology, Inc, United Kingdom) and data storage and analyzing system (software). The GMRP sample is located between two copper electrodes. The two copper electrodes are fixed on the rotor and the substratum of the rheometer by an insulating glue. The rheometer can supply a uniform magnetic field from 0 mT to 800 mT. At the same time, the distance between two copper electrodes and the normal force on the GMRP samples can be accurately controlled and measured. The modulab MTS can supply a direct voltage excitation and measure the responsive current. Finally, all the data will be saved in the data storage and analyzing system.

In our experiment, the distance between two copper electrodes was set as 1 mm, and the diameter of GMRP sample was kept as 20 mm. All samples were treated under a 780 mT magnetic field for more than 300 s as a pre-configuration process before resistance testing. The direct voltage was set as 4 V and the resistance of the copper electrode and the wire is less than 1 Ω. During the test, the time of each measurement point was set as 1 s. All the measurements were implemented at room temperature.

3. Result and Discussion

3.1 Resistance of GMRPs

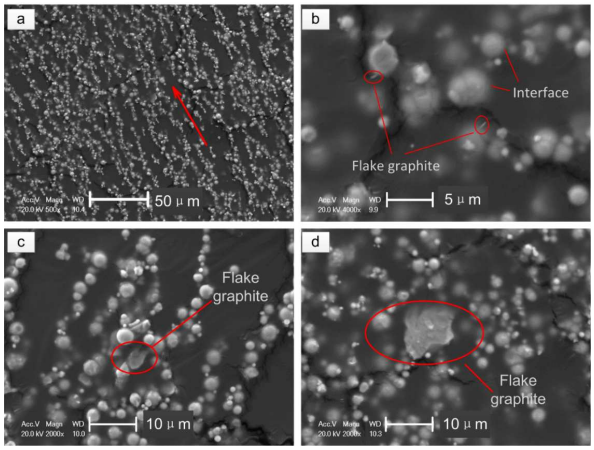

Figure 2. SEM images of GMRPs filled with different sizes FGPs after pre-configuration: (a) and (d) MRP-13.0 filled with 13.0 μm FGPs at different magnification; (b) MRP-2.6 filled with 2.6 μm FGPs; (c) MRP-6.5 filled with 6.5 μm FGPs. The weight fraction of FGP in these samples is 5%.

Figure 2 presents the SEM images of the samples after pre-configuration. It is found that almost all the CIPs are assembled to form chains-like microstructures. These chains are parallel along the direction of magnetic field (red arrow). Different from the MRE, the CIPs in the MRP are not deadly fixed in the polymer matrix, thus they cannot closely attach to each other and many interval gaps are presented. Besides the spherical CIPs, some sheet-like particles are also observed in the SEM image. These particles are indexed to be the graphite sheet. The graphite doping has not shown any significant influence on the microstructure of the final GMRPs and all the doped GMRPs with different sized graphite particles present the chains like inner structure.

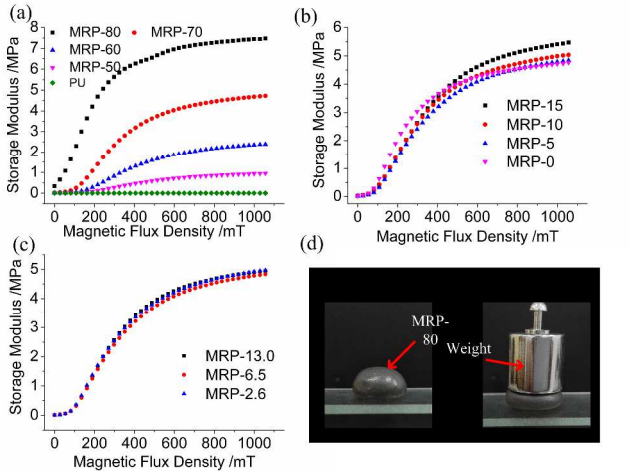

Figure 3. Storage modulus vs magnetic flux density of different GMRPs: (a) PU and GMRPs with different CIP content corresponding to 50%, 60%, 70%, 80% in weight fraction; (b) GMRPs with different FGP content corresponding to 0 wt%, 5 wt%, 10 wt%, 15 wt% in the matrix; (c) GMRPs with different FGP sizes corresponding to 13.0 μm, 6.5μm and 2.6 μm. (d) MRP-80 under a weight.

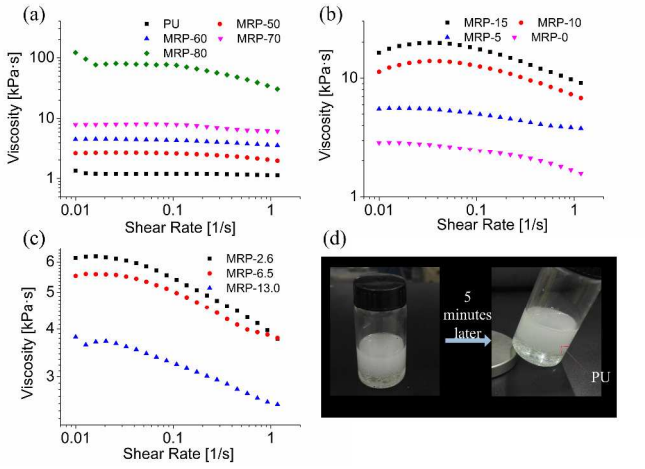

Figure 4. Viscosity vs shear rate of different GMRPs: (a) PU and GMRPs with different CIP content corresponding to 50%, 60%, 70%, 80% in weight fraction; (b) GMRPs with different FGP content corresponding to 0 wt%, 5 wt%, 10 wt%, 15 wt% in the matrix; (c) GMRPs with different FGP sizes corresponding to 13.0 μm, 6.5μm and 2.6 μm. (d) photograph of PU.

The mechanical properties of the matrix PU and the graphite doped MRP were firstly investigated. Figure 3 presents the shear storage modulus (G') of the GMRP under different magnetic flux density. Clearly, with increasing of the magnetic field, the G' increases. The saturated storage modulus is highly dependent on the content of the CIPs. As soon as the content of CIPs reaches to 80%, the storage modulus was 7.5 MPa and the relative MR

effects reached to as high as 1000%. All these results indicate the MRPs possess a high MR performance. Interestingly, the content of the graphite also exhibits an enhancing effect on the MR effects. With increasing of the graphite to 15%, the increment of the saturated storage modulus is about 0.8 MPa, this should be responded for the strengthen effects of the graphite doping. However, the storage modulus of the GMRPs doped with different sized graphite particles present a similar magnetically dependent nature, illustrates that the size of graphite particle can hardly affect the storage modulus of the graphite doped MRPs. Figure 4 gives the viscosity of GMRP with different compositions. The viscosity notably increases with the CIP content and the FGPs also exhibits a strengthen effects on the viscosity. At the same time, the size of the graphite particle only performs a weak influence on the viscosity. The high storage modulus and viscosity of GMRPs demonstrate that they are different from the traditional MR gels and MR elastomers.

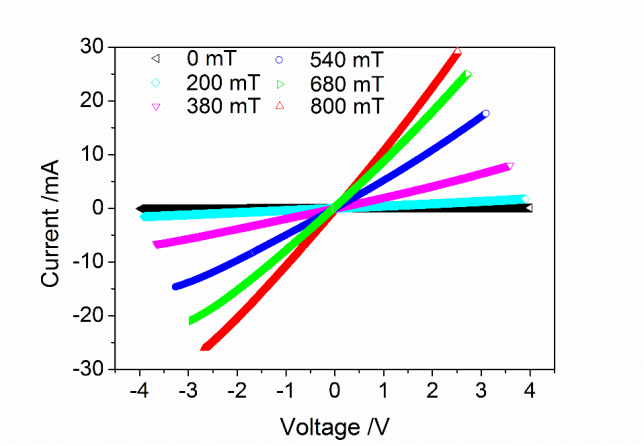

Figure 5. The I-U characteristic curve of MRP-5 under different magnetic field. The voltage linearly increased from -4 V to +4 V.

The conductive CIPs in the MRP are aggregated to chains-like microstructure, thus the MRP could be defined as a conductive materials. Figure 5 shows the I-U characteristic curve of MRP-5 under different magnetic flux density. All the curves are straight lines via the original point, which means that the resistance of GMRP can be tested by voltage dividing by current. With increasing of the magnetic flux density, the current sharply increases which illustrates that the electrical capability of the GMRPs are very sensitive to the magnetic field. Therefore, the influence of the magnetic field on the resistance of GMRP was investigated.

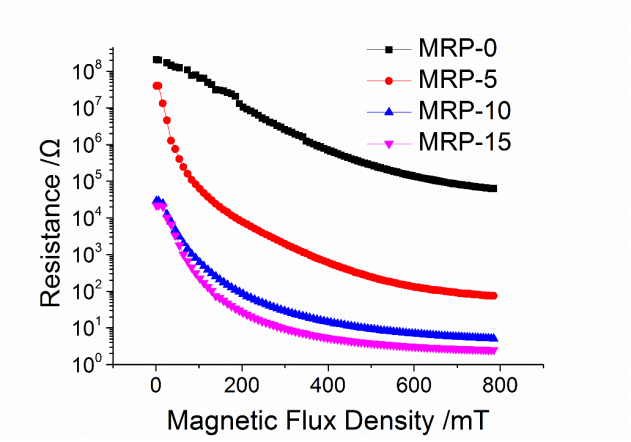

Figure 6. Resistance versus magnetic flux density of GMRPs with different FGP content. The weight fraction of FGP in the matrix of these samples are 0%, 5%, 10%, 15% respectively and the weight ratio of CIP is 70%.

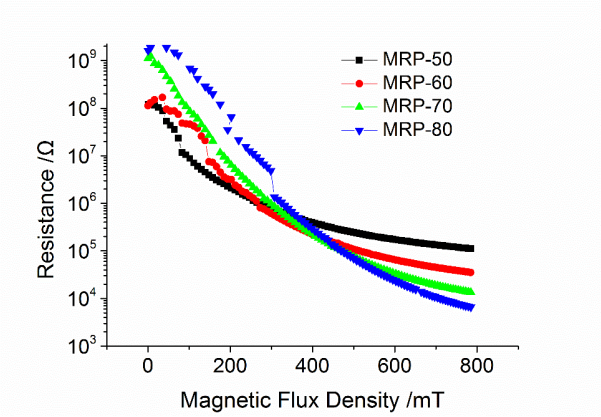

Figure 7. Resistance versus magnetic flux density of GMRPs with different CIP content. The weight fraction of CIP are 50%, 60%, 70%, 80% respectively. The weight fraction of 6.5 μm FGP in the sample is 5%

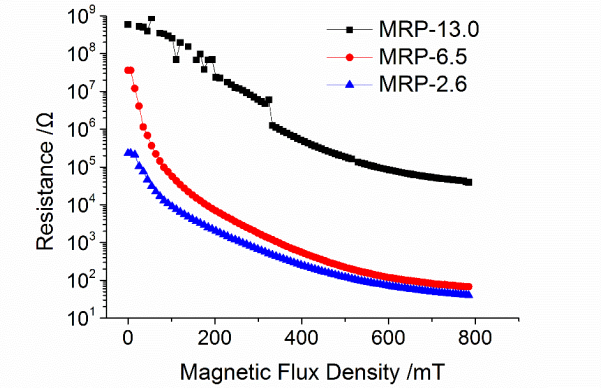

Figure 8. Resistance versus magnetic flux density of GMRPs with different FGP sizes. The weight fraction of FGP is 5% and the weight ratio of CIP is 70%.

As shown in Figure 6, with the increase of magnetic field, the resistance of the MRP firstly sharply decreases within 200 mT and then tends to level off till 800 mT. Although the CIPs are aggregated to form chains structure in the GMRPs, many internal gaps are presented in the chains, thus the conductivity of the

GMRP is low. Under applying the magnetic field, the induced dipole force between CIPs enables the chains assembled more tightly. Under a 780 mT magnetic field, the resistance drops from 22 KΩ to 2.5 Ω in sample MRP-15 and the conductivity increases about 8000 times. To this end, the conductivity increases with increasing of the magnetic field.

In this work, the graphite particles were added into the MRPs to improve the conductivity. Clearly, with increasing of the graphite, the conductivity critically increases. The above results also indicate that the conductivity of the GMRP can be controlled by varying the graphite doping. If the FGP doping is 15 wt%, the resistance significantly decreases from 200 MΩ to 22 KΩ, indicating the conductivity increases as high as 10000 times. It was found that the conductivity increased sharply with the low graphite doping. As soon as the graphite content is increased to 15%, the enhancing effect sharply decreases. Therefore, this value is defined as the optimum content for the doping.

Here, the influence of the CIP content on the conductivity of the GMRP was also investigated. As shown in Figure 7, samples with higher CIP content have higher magnetoresistances and the conductivity of all the samples increases more than 1000 times with the magnetic field increases from 0 mT to 780 mT. The resistance drops from 112000 Ω to 6600 Ω at 780 mT with rising CIP content from 50% to 80%. Interestingly, without applying the magnetic field, the resistance increases with CIP content, which may be caused by the higher viscosity of sample with higher CIP content. The high viscosity of samples makes them insensitive to small magnetic field, which leads to the high resistance when the magnetic field is small. Finally, the effects of the graphite particle size on the conductivity were also studied. Figure 8 demonstrated that the smaller FGPs often lead to a smaller resistance. Under similar content, more particles are presented in the matrix for the smaller graphite particles. In this case, more inner gaps between the CIPs in the chains would be connected by the conductive particles, thus the conductivity was increased.

3.2 Theoretical Model

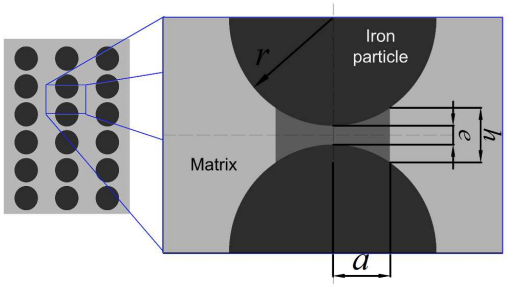

Figure 9. Sketch of particle-particle electrical resistance model. The dark spheres in the picture represent the iron particles in the sample and the light gray area represents the matrix. The dark gray area represent the area for the tunnel current.

In order to understand the conductive properties of GMRPs, a particle-particle electrical resistance model based on dipole model was developed. Here, we assume that all CIPs are of the same size and form strings one by one as shown in Figure 9. Since the resistance of the matrix is far more than that of CIPs, the resistance of GMRP mainly comes from the interface resistance between the particles, named as tunnel resistance [39]. To ensure the rationality of assumption, the microstructures of the samples were observed in Figure 3. The CIPs in the matrix attached with each other to form particle chains (Figure 9). Between the nearby two particles**,** an interface layer was found (Figure 3b) and the interface layer is composed of the polymer matrix. In this case, the resistance of the CIPs can be neglected contrasted with the tunnel resistance.

The conductivity J of tunnel current in the case of low voltage is given by [40]

$$J = [3(2m\phi)^{1/2} / 2e](E_c / d)^2 V \times \exp[-(4\pi e / d)(2m\phi_0)^{1/2}], \quad (1)$$

where m is the mass of electron, E_c is the charge of electron, Φ is the height of rectangular barrier, d is the Planck's constant and V is the voltage across film. J falls sharply with the increase of particle distance e. Therefore, we just consider the tunnel current where the particle distance is less than h. When e changes, the distance of the main contact area is still around h, so we denote the average resistivity of this area as ρ. Then the resistance of the volume unit in Figure 8 is given by

$$R = \rho \frac{e}{A}, \quad (2)$$

where A is the area of tunnel current and is given by

$$A = \pi a^2 = \pi(r^2 - (r - \frac{h-e}{2})^2) \approx \pi r(h-e). \quad (3)$$

Here e is far less than CIP radius r.

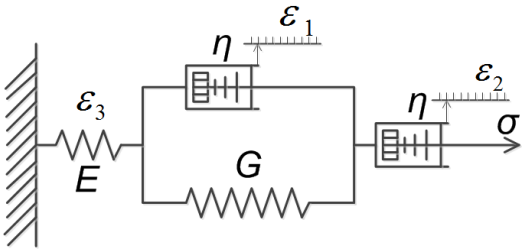

Figure 10. The four-element model used for representing the viscoelasticity interface. It is constructed by a cascade of a spring and a Voigt-Kelvin model. The Voigt-Kelvin model contains a dashpot that is parallel to a spring. Another dashpot is added for the non-crosslinked matrix.

For the plastic MR materials, the CIPs in matrix could rearrange their locations to form perfect chains under applying an external magnetic field. Therefore, the resistance would reduce in the presence of a magnetic field. In this case, the matrix is viscoelastic and the particle distance e will decrease under the dipole force between two particles. To further understand the influence of distance e on the resistance, a four-element model was proposed to represent the viscoelasticity interface. The equivalent analytical model is constructed by a cascade of a spring, a dashpot and a Voigt-Kelvin model. The Voigt-Kelvin model contains a dashpot that is parallel to a spring (Figure 10).

Using the four-element model, when the stress $\sigma = kt$, which means the stress increases linearly with time, then the relationship between the stress σ and strain ε_1 is as followed

$$\sigma = G\varepsilon_1 + \eta \frac{d\varepsilon_1}{dt}. \quad (4)$$

The solution of equation (4) is

$$\varepsilon_1(t) = \frac{kt}{G} - \frac{k\tau}{G}(1 - e^{-t/\tau}), \quad (5)$$

where $\tau = \eta/G$, named as retardation time. In our experiment, τ is far more than t, thus we reserve the first two parts of Taylor expansion of equation (5) and rewrite as

$$\varepsilon_1(t) \approx \frac{kt}{G} - \frac{k\tau}{G}(1\text{-}1\text{+}\frac{t}{\tau} - \frac{t^2}{2\tau^2}) = \frac{kt^2}{2G\tau}. \quad (6)$$

Then the variation of distance e is

$$\delta e = e_0(\varepsilon_1 + \varepsilon_2 + \varepsilon_3) \approx e_0(\frac{kt^2}{2G\tau} + \frac{\sigma t}{2\eta} + \frac{\sigma}{E}) = e_0(\frac{kt^2}{\eta} + \frac{kt}{E}). \quad (7)$$

Finally using equation (2) and (3), we obtain

$$R = \frac{\rho(1 - \frac{k}{\eta}t^2 - \frac{k}{E}t)}{\pi r(\frac{h - e_0}{e_0} + \frac{k}{\eta}t^2 + \frac{k}{E}t)}. \quad (8)$$

Hereto, we obtain the equation of the resistance of the volume unit. On the base of our assumption, the sectional area of the volume unit is given by

$$A' = \frac{\frac{4}{3}\pi r^2}{\varphi(2r + e_0)} \approx \frac{2\pi r^2}{3\varphi}. \quad (9)$$

Thus, the resistance of the sample R' is

$$R' = R \cdot \frac{H}{2r + e_0} \cdot \frac{A'}{A''} \approx \frac{\pi r H}{3\varphi A''} R, \quad (10)$$

where H is thickness of the sample, A'' is the sectional area of the sample, φ is the volume fraction of CIP. Hence, we have

$$R' = \frac{\rho H(1 - \frac{k}{\eta}t^2 - \frac{k}{E}t)}{3\varphi A''(\frac{h - e_0}{e_0} + \frac{k}{\eta}t^2 + \frac{k}{E}t)}. \quad (11)$$

In equation (11), all the parameters are fixed for a defined sample except k and t. To find out k, we first need to figure out the relationship between the dipole force F and magnetic field B. Here we do not pay much attention on how the magnetic field affect the dipole force and we just use common equations.

Generally, the force between two CIPs in a uniform magnetic field is [41]

$$F = -\frac{3\mu_0 m^2}{2\pi\mu_p r^5} = k_1 m^2, \quad (12)$$

where m is the magnetic moment of the particle. Usually the CIPs will be saturation with the increasing of the magnetic field, and then we used a fitting equation

$$M = k_2 B^{1/2}. \quad (13)$$

Therefore, we get

$$F = k_1(k_2 B^{1/2})^2 = k_f B. \quad (14)$$

Table 2 shows the k_f of all samples and the fitting curves can be found in figure S1.

Table 2. The corresponding liner fit results k_f of different samples.

Sample	MRP-50	MRP-60	MRP-70	MRP-80
k_f （N /mT）	0.0046	0.0081	0.023	0.024
Sample	MRP-0	MRP-5	MRP-10	MRP-15
k_f （N /mT）	0.019	0.017	0.021	0.018
Sample	MRP-13.0	MRP-6.5	MRP-2.6	
k_f （N /mT）	0.024	0.016	0.020	

In our experiment, the increase rate of the magnetic field was kept at 7.8 mT/s. The relationship between F and σ is

$$\sigma = \frac{F}{A''} \cdot \frac{A'}{\pi r^2} \approx \frac{2F}{3\varphi A''}. \quad (15)$$

Thus, we can get

$$k = \frac{5.2k_f}{\varphi A''}. \quad (16)$$

SEM analysis demonstrates that the FGPs are randomly dispersed in the polymer matrix. FGPs are nonmagnetic materials and the magnetic field cannot influence the position of FGPs directly, but the experimental results shows that the resistance of MRPs will change a lot by FGPs. To understand the effects of the flake graphite particles on the resistance, the parameter α was introduced to show the effect of flake graphite and we set. α as unit value 1 when there is no FGPs in the sample. Finally using equation (11) we get

$$R' = \frac{\rho H(1 - \frac{5.2k_f}{\varphi A''\eta}t^2 - \frac{5.2k_f}{\varphi A''E}t)}{3\alpha\varphi A''(\frac{h - e_0}{e_0} + \frac{5.2k_f}{\varphi A''\eta}t^2 + \frac{5.2k_f}{\varphi A''E}t)}. \quad (17)$$

In equation (17), some parameters are constant, we substitute these parameters and thus obtain

$$R' = \frac{1.06\rho(1 - \frac{16600k_f}{\varphi\eta}t^2 - \frac{16600k_f}{\varphi E}t)}{\alpha\varphi(\frac{h - e_0}{e_0} + \frac{16600k_f}{\varphi\eta}t^2 + \frac{16600k_f}{\varphi E})}, \quad (18)$$

or

$$R' = \frac{1.06\rho(1 - \frac{280k_f}{\varphi\eta}B^2 - \frac{2100k_f}{\varphi E}B)}{\alpha\varphi(\frac{h - e_0}{e_0} + \frac{280k_f}{\varphi\eta}B^2 + \frac{2100k_f}{\varphi E}B)}. \quad (19)$$

In equation (18) and (19), ρ, η and E are calibration values and these parameters are constant once confirmed.

3.3 Theoretical Result and Analysis

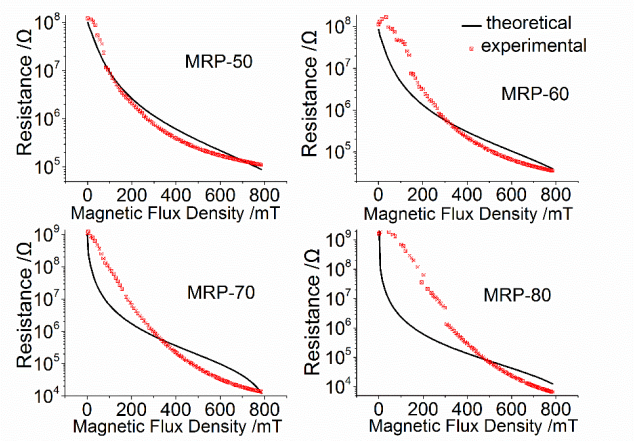

Figure 11. Comparison of theoretical and experimental results of samples with different CIP content. The CIP weight ratio of these samples are 50%, 60%, 70% and 80% respectively.

Table 3. The relevant fitting parameters: relative initial particle distance and α used in the theoretical model.

Sample	MRP-50	MRP-60	MRP-70	MRP-80
$(h\text{-}e_0)/e_0$	0.0005	0.00035	0.00008	0.00001
α	4479	5119	1333	3626

Figure 11 shows the comparison of theoretical and experimental results of samples with different CIP content and Table 3 exhibits the relevant fitting parameters. Clearly, the theoretical results match the experimental results well when the CIP content of sample is less than 70%. If the amount of the CIPs is too high, complex aggregation structures will be formed. In this case, the proposed model was not proper. Moreover, for MRP-80, the error of k_f cannot be neglected. The relative initial particle distance ($(h-e_0)/e_0$) decrease with the increase of CIP content (Table 3) and the viscosity increases with the rise of CIP content. In a higher viscosity matrix, the CIPs meet higher constraint force during the pre-configuration process and the rearrange process becomes more difficult. No critical difference was found for the parameter α, illustrating that the FGPs and CIPs influence the resistance separately.

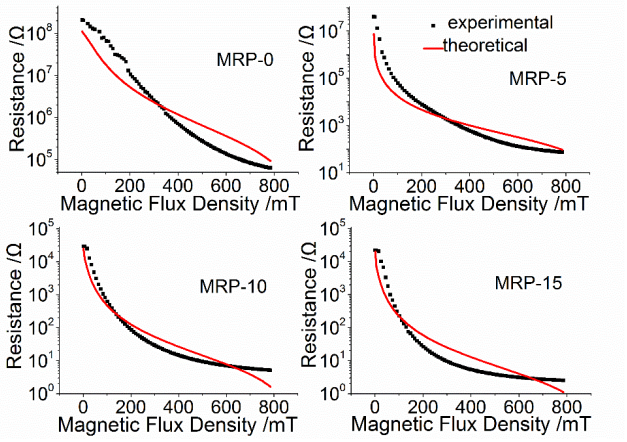

Figure 12. Comparison of theoretical and experimental results of samples with different FGP content. The weight ratio of FGP in the matrix are 0%, 5%, 10% and 15% respectively and the weight fraction of CIP in these samples is 70%.

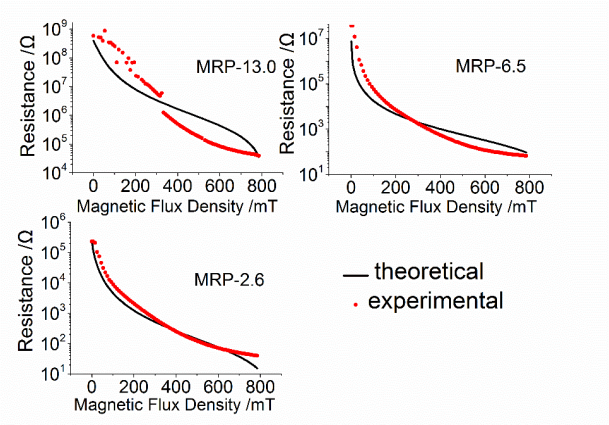

Figure 13. Comparison of theoretical and experimental results of samples with different FGP sizes. Their weight ratio of FGP in the matrix are 5%, and the weight fraction of CIP in these samples is 70%.

Figure 12 and Figure 13 show the magnetic field dependent resistance of the MRP with different FGP content and sizes. The theoretical results match well with the experimental results. The deviation between the theoretical results and the experimental results becomes larger when the magnetic field is larger than 500 mT. Because the particle distance e cannot reduce forever and it has a limitation with increasing of the magnetic field, the resistance will gradually level off.

Table4. The relevant fitting parameter α used in the theoretical model.

Sample	MRP-0	MRP-5	MRP-10	MRP-15
α	1	1333	40000	100000
Sample	MRP-13.0	MRP-6.5	MRP-2.6	
α	0.5	1333	4000	

The factors α for FGPs are listed in Table 4. The factor α increases sharply with the rising of FGP content, which means the resistance can be tremendously decreased by adding FGPs in the matrix. Meanwhile, the factor α increases with the decrease of the FGP size.

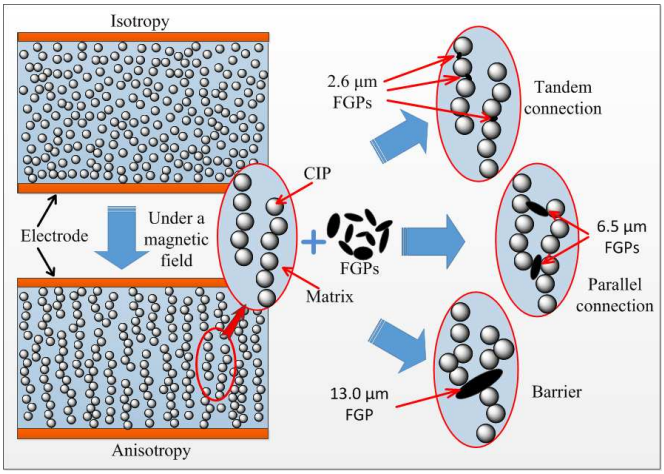

Figure 14. Schematic of the conductivity improving mechanism of the graphite doped MRP under a magnetic field.

To further analyze the conductive characteristics of the GMRP, a possible mechanism was proposed (Figure 14). In this work, the FGPs work like bridges to connect the conductive chains in the matrix. Without the magnetic field, CIPs and FGPs are loosely dispersed in the matrix. The gap between the particles is so large that few channel for the current is presented in the materials. As soon as a magnetic field is applied, the iron particles tend to aggregate much closer under driven of the dipole force between iron particles. Therefore, the conductivity of GMRP sharply increased with increasing of the magnetic field. Here, many defects were present in the CIP chains and some of them are of low conductivity. The graphite flasks are conductive and they can uniformly disperse in the polymer matrix. They can also bridge the non-contact particle chains thus improve the conductivity. With increasing of the number of the graphite particles, the conductivity increases. Therefore, the resistance of the GMRP decreases with decreasing the size of the graphite particles.

Similarly, the resistances sharply decrease with the increase of FGPs content of GMRPs.

Based on the above analysis, we can find that the conductivity of the GMRP is highly dependent on the content and size of the doped graphite particle. In consideration of the magnetic sensitivity, the GMRP are promising for practical application as the magnetic field sensor or magnetically controllable on-off switch.

3.4 Magnetically controllable on-off switch

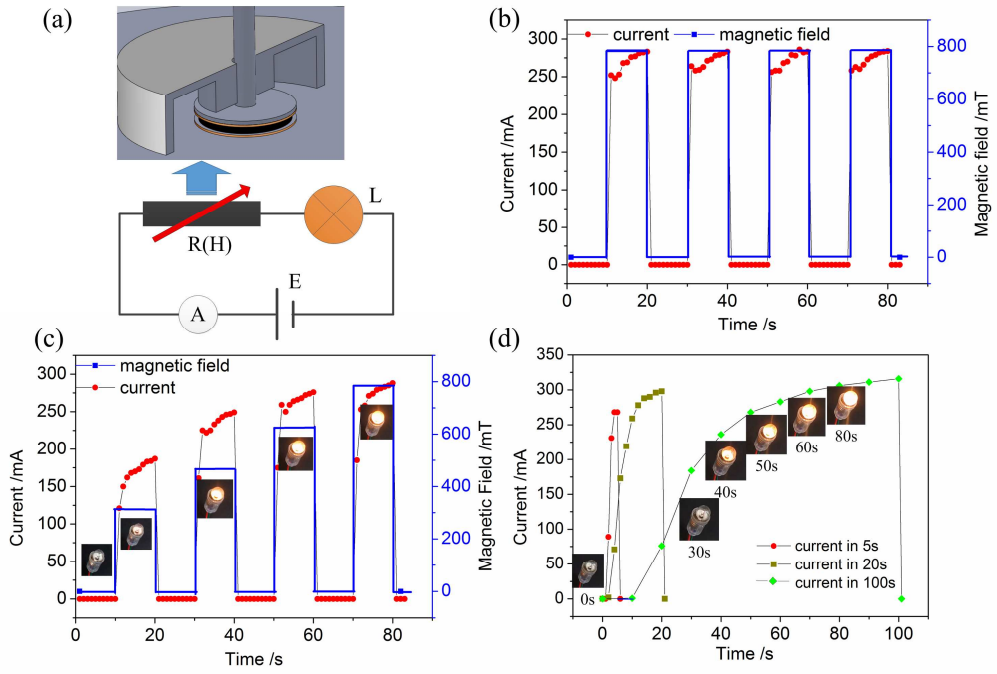

Figure 15. (a) Schematic illustration of devices in the experiment containing a magnetic on-off switch; conductive capability of sample MRP-15 and luminance of bulb change in terms of time under different magnetic field: (b) a square wave magnetic field, (c) a step wave magnetic field and (d) a triangular wave magnetic field with different rising time.

By utilizing the above-mentioned characteristic of the GMRP, a magnetically controllable on-off switch was constructed and its magnetic field dependent sensitivity was studied. As shown in Figure 15a, two parallel copper electrodes were attached on the surface of the GMRP to form a switch. Without applying magnetic field, the bulb were turn off. After a magnetic field was applied, the bulb became bright. Figure 15b showed the time dependent current in the circuit upon a square wave magnetic field. It was found that the current increased quickly (within 1s) as soon as the magnetic field was added. Similarly, once the magnetic field was withdrawn, the current decreased to zero, which indicated a quick response of our repeated on-off switch.

Different from the previously reported quick response switch, the sensing current and response time could be tuned by varying the magnetic field. As show in Figure 15c, under a step wave magnetic field, the bulb became bright at the wave crest of magnetic field and its luminance increases with the increase of magnetic field. It means that the sensing current can be controlled by adjusting the magnetic field. Moreover, the turn on process could also be controlled by adjusting the increasing rate of magnetic field. Figure14d shows the time dependence of current by slowly increasing the magnetic field. We control the growth speed of magnetic field and make sure that the magnetic field uniformly increased from 0 mT to 780 mT in 5 s, 20 s and 100 s respectively. As shown in the picture, the current slowly increased to the maximum in different times corresponding to the growth speed of magnetic field. Clearly, the on-off time was tunable by varying the magnetic field and the light-emission change of the bulb in Figure 15d showed the turn on process directly. This advantage enable the on-off switch be widely applied in the smart device by protecting the electronics from destroyed by quick and large electro-current.

4. Conclusions

In this work, graphite particles were introduced into MRP to improve the electro-conductivity of the final GMRPs. The influence of the content and size of the graphite particle on the resistance of GMRP was investigated. The experimental results showed that the resistance of non-doped MRP was approximately 10000 times higher than the resistance of sample MRP-15 with 15 wt% graphite doping. Meanwhile, the conductivity of the GMRP was magnetically sensitive and they increased more than three orders with the magnetic field increasing from 0 mT to 780 mT. A particle-particle electrical resistance model based on dipole model was developed to understand the improving mechanism and the theoretical results matched the experimental results well. At last, a magnetic field controlled on-off switch based on GMRP was developed and the results demonstrated that

the current in the circuit increased quickly according to the external magnetic field and their sensing time was tunable by varying the increasing velocity of the magnetic field.

Acknowledgements

The financial support of the National Natural Science Foundation of China (Grant Nos. 11125210) and the Anhui Provincial Natural Science Foundation of China (1408085QA17) are gratefully acknowledged. This work was also supported by Collaborative Innovation Center of Suzhou Nano Science and Technology.

Notes and references

[a] *CAS Key Laboratory of Mechanical Behavior and Design of Materials, Department of Modern Mechanics, University of Science and Technology of China, Hefei, 230027, P. R. China. Fax & Tel: +86 551 63600419; E-mail: gongxl@ustc.edu.cn (Xinglong Gong) and xuansh@ustc.edu.cn (Shouhu Xuan)*

1 Y. G. Xu, X. L. Gong, S. H. Xuan, W. Zhang and Y. C. Fan, *Soft Matter*, 2011, **7**, 5246.
2 S. H. Xuan, Y. L. Zhang, Y. F. Zhou, W. Q. Jiang and X. L. Gong, *J Mater Chem*, 2012, **22**, 13395-13400.
3 J. de Vicente, D. J. Klingenberg and R. Hidalgo-Alvarez, *Soft Matter*, 2011, **7**, 3701-3710.
4 Y. Tian, M. L. Zhang, J. L. Jiang, N. Pesika, H. B. Zeng, J. Israelachvili, Y. G. Meng and S. Z. Wen, *Phys Rev E*, 2011, **83**.
5 S. H. Piao, M. Bhaumik, A. Maity and H. J. Choi, *J Mater Chem C*, 2015, **3**, 1861-1868.
6 M. R. Jolly, J. D. Carlson, B. C. Munoz and T. A. Bullions, *J Intel Mat Syst Str*, 1996, **7**, 613-622.
7 J. M. Ginder, S. M. Clark, W. F. Schlotter and M. E. Nichols, *Int J Mod Phys B*, 2002, **16**, 2412-2418.
8 T. Mitsumata and S. Ohori, *Polym Chem-Uk*, 2011, **2**, 1063-1067.
9 Y. C. Li, J. C. Li, W. H. Li and H. P. Du, *Smart Materials and Structures*, 2014, **23**.
10 T. X. Liu, X. L. Gong, Y. G. Xu, H. M. Pang and S. H. Xuan, Smart Materials and Structures, 2014, 23.
11 W. L. Hu, R. R. Wang, Y. F. Lu and Q. B. Pei, *J Mater Chem C*, 2014, **2**, 1298-1305.
12 S. Sayyar, E. Murray, B. C. Thompson, J. Chung, D. L. Officer, S. Gambhir, G. M. Spinks and G. G. Wallace, *J Mater Chem B*, 2015, **3**, 481-490.
13 A. Celzard, J. F. Mareche, F. Payot and G. Furdin, Carbon, 2002, 40, 2801-2815.
14 S. Kim, J. Byun, S. Choi, D. Kim, T. Kim, S. Chung and Y. Hong, Adv Mater, 2014, 26, 3094-3099.
15 G. Ausanio, V. Iannotti, E. Ricciardi, L. Lanotte and L. Lanotte, Sensor Actuat a-Phys, 2014, 205, 235-239.
16 J. E. Martin, R. A. Anderson, J. Odinek, D. Adolf and J. Williamson, Phys Rev B, 2003, 67.
17 J. E. Martin, E. Venturini, J. Odinek and R. A. Anderson, Phys Rev E, 2000, 61, 2818-2830.
18 N. Kchit and G. Bossis, J Phys D Appl Phys, 2009, 42.
19 X. J. Wang, F. Gordaninejad, M. Calgar, Y. M. Liu, J. Sutrisno and A. Fuchs, J Mech Design, 2009, 131.
20 N. Ghafoorianfar, X. J. Wang and F. Gordaninejad, Smart Materials and Structures, 2014, 23.
21 Y. G. Xu, X. L. Gong, T. X. Liu and S. H. Xuan, Soft Matter, 2013, 9, 7701-7709.
22 M. Yu, B. X. Ju, J. Fu, S. Z. Liu and S. B. Choi, Ind Eng Chem Res, 2014, 53, 4704-4710.
23 I. Bica, Mater Lett, 2009, 63, 2230-2232.
24 N. Kchit, P. Lancon and G. Bossis, J Phys D Appl Phys, 2009, 42.
25 J. L. Mietta, M. M. Ruiz, P. S. Antonel, O. E. Perez, A. Butera, G. Jorge and R. M. Negri, Langmuir, 2012, 28, 6985-6996.
26 T. F. Tian, W. H. Li, G. Alici, H. Du and Y. M. Deng, Rheol Acta, 2011, 50, 825-836.
27 T. F. Tian, W. H. Li and Y. M. Deng, Smart Mater Struct, 2011, 20.
28 I. Bica, Y. D. Liu and H. J. Choi, Colloid Polym Sci, 2012, 290, 1115-1122.
29 M. Q. Sun, G. C. Wang, C. Y. Yang, H. Jiang and C. Z. Li, *J Mater Chem A*, 2015, **3**, 3880-3890.
30 S. T. Hsiao, H. W. Tien, W. H. Liao, Y. S. Wang, S. M. Li, C. C. MMa, Y. H. Yu and W. P. Chuang, *J Mater Chem C*, 2014, **2**, 7284-7291.
31 J. C. Ribot, C. Guerrero-Sanchez, T. L. Greaves, D. F. Kennedy, R. Hoogenboom and U. S. Schubert, *Soft Matter*, 2012, 8, 1025-1032.
32 J. C. Ribot, C. Guerrero-Sanchez, R. Hoogenboom and U. S. Schubert, *J Mater Chem*, 2010, **20**, 8279-8284.
33 J. C. Ribot, C. Guerrero-Sanchez, R. Hoogenboom and U. S. Schubert, *Chem Commun*, 2010, **46**, 6971-6973.
34 C. Guerrero-Sanchez, T. Lara-Ceniceros, E. Jimenez-Regalado, M. Rasa and U. S. Schubert, *Adv Mater*, 2007, **19**, 1740-1747.
35 C. Guerrero-Sanchez, C. Fabrie and U. S. Schubert, Magnetorheological solid composites based on ionic liquids, 2009.
36 T. L. Belenkova, D. Rimmerman, E. Mentovich, H. Gilon, N. Hendler, S. Richter and G. Markovich, *J Mater Chem*, 2012, **22**, 24042-24047.
37 K. Fic, E. Frackowiak and F. Beguin, *J Mater Chem*, 2012, **22**, 24213-24223.
38 J. Jiu, M. Nogi, T. Sugahara, T. Tokuno, T. Araki, N. Komoda, K. Suganuma, H. Uchida and K. Shinozaki, *J Mater Chem*, 2012, **22**, 23561-23567.
39 L. Kogut and K. Komvopoulos, *J Appl Phys*, 2003, 94, 3153-3162.
40 J. G. Simmons, *J Appl Phys*, 1963, 34, 2581-2590.
41 L. Rodriguez-Arco, M. T. Lopez-Lopez, A. Y. Zubarev, K. Gdula and J. D. G. Duran, *Soft Matter*, 2014, 10, 6256-6265.